J. Phys.: Condens. Matter **9** (1997) 8085–8100. Printed in the UK PII: S0953-8984(97)80830-2

Current-driven vortex dynamics in untwinned $YBa_2Cu_3O_7$ superconducting single crystals

W Jiang†, N-C Yeh†, T A Tombrello†, A P Rice† and F Holtzberg‡

† Department of Physics, California Institute of Technology, Pasadena, CA 91125, USA
‡ IBM, Thomas J Watson Research Center, Yorktown Heights, NY 10598, USA

Received 10 January 1997, in final form 1 July 1997

Abstract. Current-driven vortex dynamics of type-II superconductors in the weak-pinning limit is investigated by quantitatively studying the current-dependent vortex dissipation of an untwinned $YBa_2Cu_3O_7$ single crystal. For applied current densities (J) substantially larger than the critical current density (J_c), non-linear resistive peaks appear below the thermodynamic first-order vortex-lattice melting transition temperature (T_M), in contrast to the resistive hysteresis in the low-current limit ($J < J_c$). These resistive peaks are quantitatively analysed in terms of the current-driven coherent and plastic motion of vortex bundles in the vortex-solid phase, and the non-linear current–voltage characteristics are found to be consistent with the collective flux-creep model. The effects of high-density random point defects on the vortex dynamics are also investigated via proton irradiation of the same single crystal. Neither resistive hysteresis at low currents nor peak effects at high currents are found after the irradiation. Furthermore, the current–voltage characteristics within the instrumental resolution become completely ohmic over a wide range of currents and temperatures, despite theoretical predictions of much larger J_c-values for the given experimental variables. This finding suggests that the vortex-glass phase, a theoretically proposed low-temperature vortex state which is stabilized by point disorder and has a vanishing resistivity, may become unstable under applied currents significantly smaller than the theoretically predicted J_c. More investigation appears necessary in order to resolve this puzzling issue.

1. Introduction

Recent experimental observations of novel vortex transport properties in various weak-pinning type-II superconductors [1–10] have kindled renewed interest in the effects of static disorder on the thermodynamic vortex phases and phase transitions [11–16]. In the weak-pinning limit, measurements of thermodynamic quantities such as magnetization and heat capacity have confirmed the existence of a first-order melting transition in both $Bi_2Sr_2CaCu_2O_x$ [9] and untwinned $YBa_2Cu_3O_7$ single crystals [10], while the resistive hysteresis observed in untwinned $YBa_2Cu_3O_7$ single crystals below the first-order vortex-solid melting transition temperature T_M [1–3] has been attributed to the current-driven non-equilibrium effects below the thermodynamic transition [3]. Another current-induced phenomenon in weak-pinning systems is the 'peak effect', which refers to a peak feature in the critical current density (J_c) as a function of the temperature or magnetic field [17–21]. The peak effect has been observed just below the upper critical field $H_{c2}(T)$ in conventional superconductors such as niobium [17] and Nb_3Ge films [18], and has been attributed to the softening of the elastic moduli in the vortex lattice first by Pippard [19] and then in a generalized way by Larkin and Ovchinnikov [20]. Recently similar peak effects

0953-8984/97/388085+16$19.50

have been reported for conventional superconductors such as 2H-$NbSe_2$ single crystals [4], and for high-temperature superconductors (HTSs) such as $YBa_2Cu_3O_7$ single crystals either with very few twin boundaries [5, 6] or completely untwinned [7]. In the case of high-temperature superconductors, it has been theoretically argued that the peak effect occurs just below the vortex-solid melting line $H_M(T)$ rather than near $H_{c2}(T)$ [15], because the shear modulus c_{66} in HTSs vanishes at H_M [3, 15] due to large thermal fluctuations, and the rapid decrease of c_{66} associated with the softening vortex solid below $H_M(T)$ is known to result in enhancement of the pinning and therefore the peak effect in the critical current density J_c [15, 19–21].

In this paper, we report our quantitative investigations of the current-driven vortex dynamics in the weak-pinning limit by studying an untwinned $YBa_2Cu_3O_7$ single crystal. We find that below the temperature where the peak of J_c occurs, the non-linear current–voltage characteristics can be described in terms of the collective flux-creep model [15, 22, 23]. In addition, both coherent and plastic motion of vortex bundles in the high-current limit are proposed to account for the peak effect in J_c. We also investigate the effect of high-density point defects on the low-temperature vortex phase and on the nature of the vortex phase transition by means of proton irradiation of the same untwinned single crystal. We find that the crystal, after proton irradiation, exhibits completely ohmic current–voltage characteristics over a wide current range. Furthermore, neither resistive hysteresis nor a peak effect is present after irradiation, suggesting that the low-temperature vortex state is unstable against finite currents in the presence of high-density random point defects, and that the scenario for a point-disorder-induced vortex-glass state at low temperatures [11] needs further careful examination.

2. Experimental procedure

The sample studied in this work was an untwinned $YBa_2Cu_3O_7$ single crystal with dimensions of 0.5 mm $\times$ 0.5 mm $\times$ 20 μm, the same as was used in our previous resistive hysteresis studies [3]. The onset of the superconductivity was at $T_c = 93.44 \pm 0.03$ K and the normal-state b-axis resistivity was $\rho_n(T_c) = 25\ \mu\Omega$ cm at T_c. The dc current–voltage characteristics were measured using a standard four-terminal method. The measurements were performed in applied magnetic fields (H) from 1 to 90 kOe and for angles (θ) from 0° to 90°, where θ is defined as the angle between the applied field and the sample c-axis. The applied current density $\boldsymbol{J}$ was always transverse to $\boldsymbol{H}$ and parallel to the crystalline b-axis. The resistivity, defined as $\rho \equiv E/J$, was obtained from the electric field versus current density (E–J) isotherms. The voltage resolution was ~50 nV, and the range of the current density was from 10^3 A m^{-2} to 10^7 A m^{-2}. The same sample was subsequently irradiated with 3.0 MeV protons using a fluence of 5×10^{15} protons cm^{-2}, and the irradiation resulted in point and small cluster defects of a volume density $n_p \sim (3 \times 10^{-8}\ \mathrm{m})^{-3}$ [24, 25]. Similar measurements of the resistivity and the current–voltage characteristics were performed to investigate the effects of high-density random point disorder on the vortex dynamics.

3. Results

Illustrated in figure 1 are the temperature-dependent resistivity curves taken with different applied currents near the vortex-solid melting transition and for $H = 50$ kOe and $\theta = 0°$. In the low-current limit ($J < 1.5 \times 10^5$ A m^{-2}), the ρ–T curves exhibit hysteretic behaviour (not shown in figure 1) upon cooling and heating, as reported previously [3]. However,

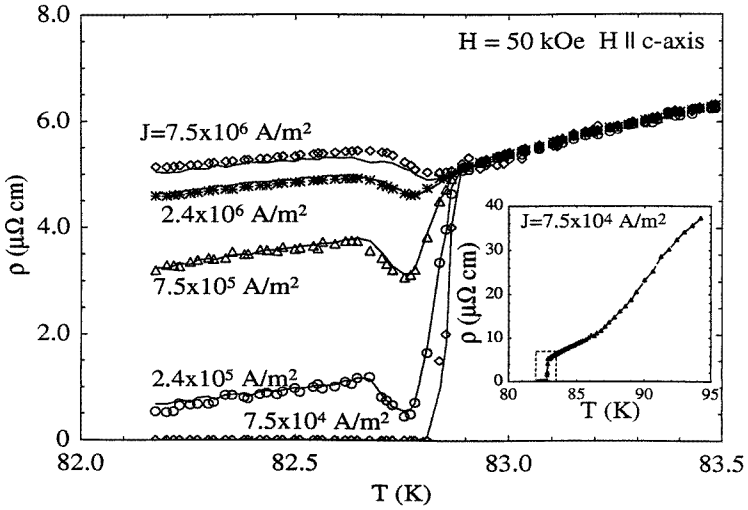

Figure 1. Non-linear resistivity (ρ) versus temperature (T) curves of the as-grown untwinned $YBa_2Cu_3O_7$ single crystal taken at different current densities and for $H = 50$ kOe, and for $\boldsymbol{H} \parallel \hat{c}$. The solid lines are the theoretical fitting curves obtained using equation (1) and with $\mu = 1.28$. The inset shows the ohmic ρ–T curve over a larger temperature range and taken at $J = 7.5$ A cm^{-2}. The box indicates the temperature window shown in the main figure.

for higher current densities ($J > 1.5 \times 10^5$ A m^{-2}), the hysteretic behaviour gradually disappears, and a resistive peak occurs and becomes more pronounced with increasing J until $J \sim 2.4 \times 10^6$ A m^{-2}. We note that both a peak and a 'dip' in the resistivity occur at temperatures lower than the thermodynamic vortex-solid melting temperature T_M, where T_M has been identified according to reference [3]. The non-linear vortex response near the peak region is further illustrated by the electric field (E) versus current density (J) isotherms in figure 2(a) for $H = 50$ kOe and $\boldsymbol{H} \parallel \hat{c}$. We note that the temperature interval within which the current-dependent resistive peaks occur (see figure 1) corresponds to the occurrence of non-linear E–J isotherms in figure 2(a). In general, the peak effect always exists if $H < 90$ kOe for fields along the c-axis. On the other hand, for fields in the ab-plane the peak effect can be observed only if $H \geqslant 10$ kOe.

4. Analyses using the collective flux-creep model

To obtain a better understanding of the E–J characteristics, we examine the low-temperature E–J isotherms which show vanishing resistivity as $J \to 0$. This non-linear behaviour is consistent with the bundle-hopping resistivity of vortices proposed by the collective flux-creep model [15, 22]:

$$\rho(T, J) = \rho_0(T) \exp\left[-\left(\frac{J_{vb}(T)}{J}\right)^{\mu}\right] \tag{1}$$

where J_{vb} is a characteristic current density related to the correlation length of vortex bundles, and μ is a positive exponent. Assuming that the exponent μ is constant for given H and θ, we apply equation (1) to our data by using the fitting parameters μ, $\rho_0(T)$ and $J_{vb}(T)$, and find that the resistivity agrees well with the collective flux-creep model. We note that $\mu > 0$ yields a vanishing resistivity in the small-current limit. As a demonstration,

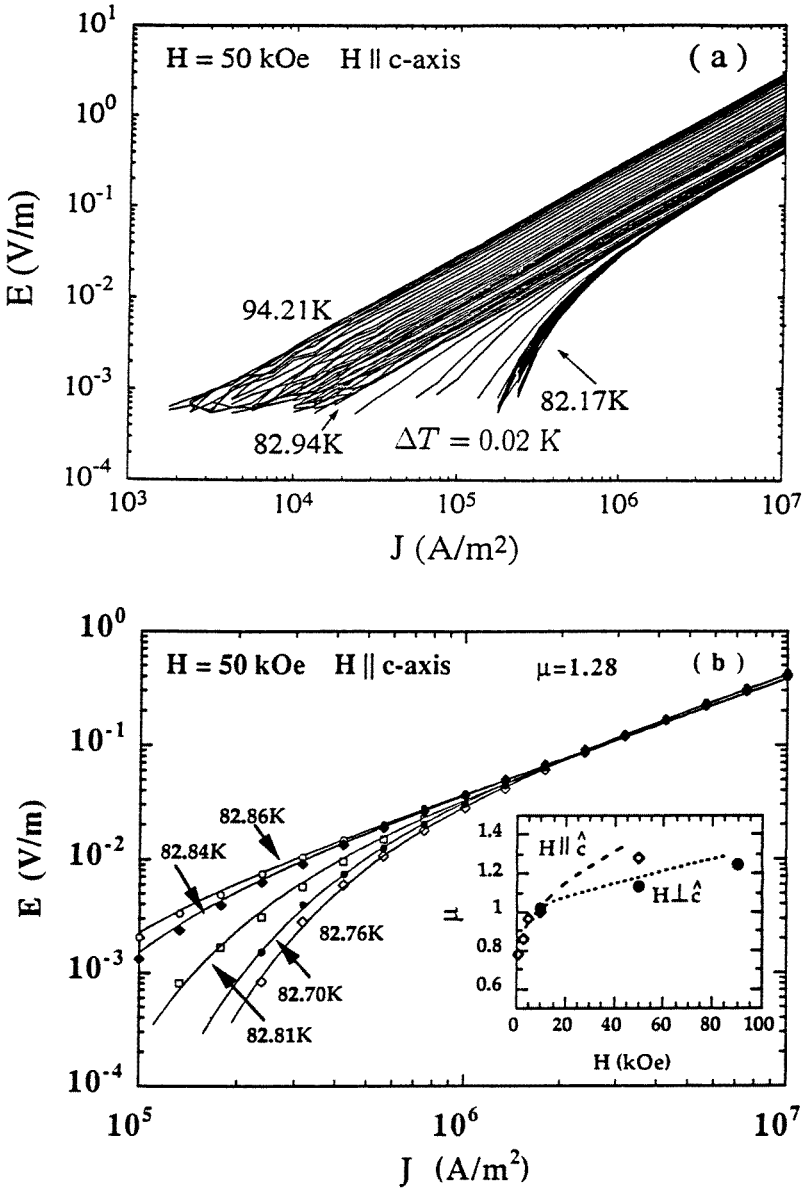

Figure 2. (a) A representative set of electric field (E) versus current density (J) isotherms for the sample for $H = 50$ kOe and $\boldsymbol{H} \parallel \hat{c}$. The temperature increment ΔT of two consecutive isotherms is 0.02 K within the region indicated by the arrows. (b) Representative theoretical fitting curves (solid lines) for the E–J isotherms obtained with the use of the collective flux-creep model of equation (1) and a fitting parameter $\mu = 1.28$. The inset shows the μ-values for different magnetic fields and orientations. (c) Representative theoretical fitting curves (solid lines) for the E–J isotherms, obtained using the empirical formula $E \propto (J - J_c)^{\alpha}$.

five representative E–J fitting curves are plotted as solid lines in figure 2(b) together with the original data points for $H = 50$ kOe and $\theta = 0^{\circ}$. In addition, the solid lines in figure 1 are also fitting curves for the $\rho(T, J)$–T data, obtained with the use of equation (1). The

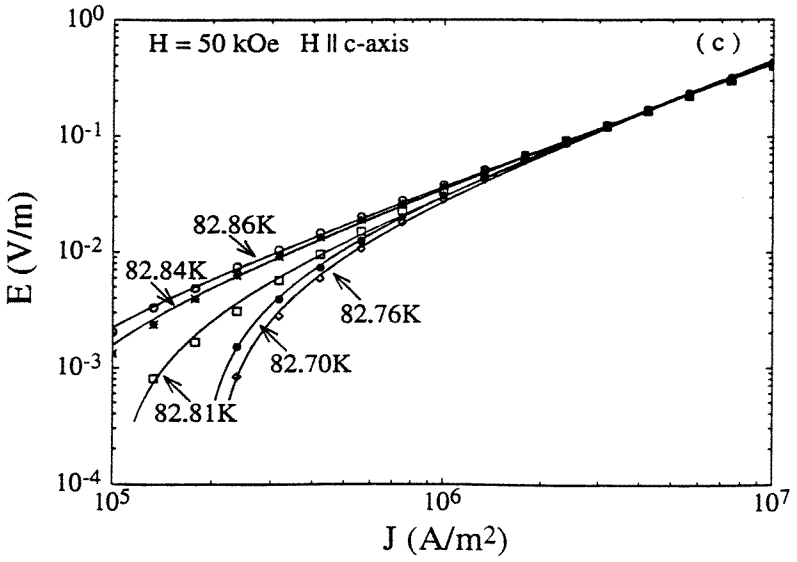

Figure 2. (Continued)

μ-values thus determined are shown in the inset of figure 2(b) for the results taken with both $\boldsymbol{H} \parallel \hat{\boldsymbol{c}}$ and $\boldsymbol{H} \perp \hat{\boldsymbol{c}}$. According to the collective flux-creep model [22, 23], the magnitude of μ varies with the range of vortex correlation. Although the accuracy of the μ-values is limited by the finite current range of our experiments, all of the μ-values derived from the E–J data fall between the theoretical values of $\frac{7}{9}$ for large vortex bundles and $\frac{5}{2}$ for small vortex bundles, in general agreement with the collective flux-creep model [22, 23].

In addition to the exponent μ described above, the quantities $\rho_0(T)$ and $J_{vb}(T)$ are worth considering. We note that the expression $\lim_{J \gg J_{vb}}[\rho(T, J)] = \rho_0(T)$ holds according to equation (1), and that $\rho_0(T)$ has a temperature dependence that is similar to but much weaker than $\rho(T)$, as shown in figure 3(a). Furthermore, the characteristic current density $J_{vb}(T)$ illustrated in figure 3(b) shows a distinct peak at the temperature where a minimum in $\rho(T)$ occurs. This temperature dependence of $J_{vb}(T)$ is analogous to the behaviour of the critical current density J_c [6], where J_c is determined according to the empirical relation $E(J) \propto [J - J_c(T)]^{\alpha}$, with α being a temperature-dependent exponent, where $J_c(T) \to 0$ and $\alpha(T) \to 1$ as $T \to T_M^-$. The resulting $J_c(T)$ curves are shown in figure 3(b), and the corresponding fitting curves for the E–J data are shown in figure 2(c). We note that both the expression given as equation (1) and the empirical relation $E \propto [J - J_c(T)]^{\alpha}$ are consistent with our attribution of the dissipation below T_M to the current-driven vortex motion in the vortex-solid state, because both J_{vb} and J_c are finite only if $T < T_M$. It is also interesting to compare our empirical relation with the current–voltage characteristics of charge-density-wave (CDW) behaviour in the mean-field approximation for a strong-pinning system, where $E \propto [J - J_c]^{3/2}$ is satisfied [26]. Such behaviour has been reported for $YBa_2Cu_3O_7$ melt-textured samples and twinned crystals [21] where significant pinning defects are present. Although the mean-field CDW behaviour is similar to our current–voltage characteristics, we note that the power α for our untwinned single crystal is always smaller than 3/2 for all of the temperatures of our investigation. This difference may be attributed to the weak-pinning nature of the untwinned $YBa_2Cu_3O_7$ single crystal.

The correlation between J_{vb} and J_c can be understood in the context of the collective

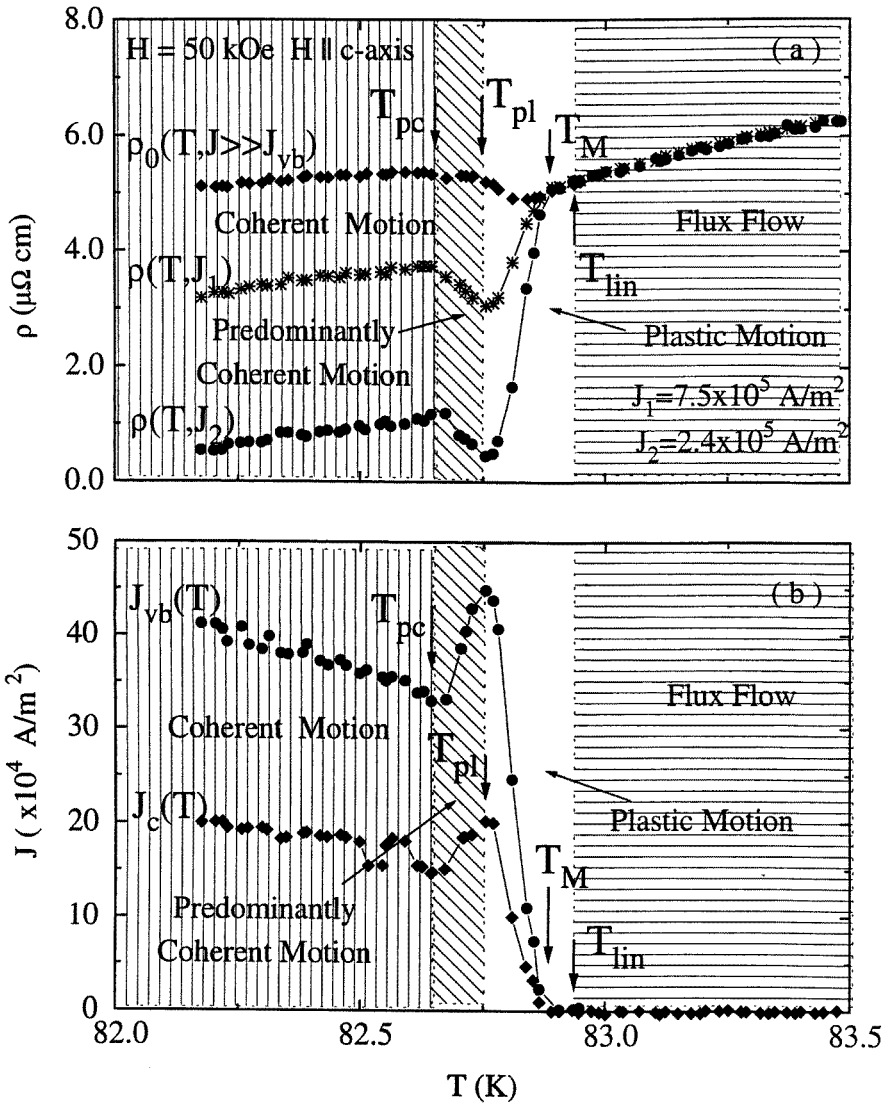

Figure 3. Representative data for (a) the ρ_0–T and ρ–T curves for $H = 50$ kOe and $\boldsymbol{H} \parallel \hat{c}$ are compared with (b) the corresponding $J_{vb}(T)$ and $J_c(T)$ data. Note the strong correlations between the peak feature in $\rho(T)$ and those in $J_{vb}(T)$ and $J_c(T)$. The different regimes of vortex motion are as indicated.

flux-creep theory [23] by means of the following consideration. (For simplicity, we shall ignore the electronic mass anisotropy for the time being.) In the case of small-bundles pinning, which corresponds to either small magnetic fields or large applied currents, the characteristic current is given by $J_{vb} \approx J_0(\xi/a_0)^2(a_0/L_c)^{3/5}$, where J_0 is the depairing current density, L_c is the longitudinal correlation length of the vortex bundle, and a_0 is the Abrikosov vortex-lattice constant [23]. The J_c-value near the crossover to small-bundle pinning is given by $J_c \sim J_0(\xi/a_0)^2$, according to section IV.B.1 of reference [23]. Therefore we find that $J_{vb} \approx J_c(a_0/L_c)^{3/5}$. In the case of large-bundle pinning either at

high fields or under small applied currents, it is found that $J_{vb} \approx (J_0/\kappa^2)(a_0/L_c)^{3/5}$, and J_c is approximated by $J_c \sim (J_0/\kappa^2)(a_0/L_c)^6$ [23]. Therefore we obtain $J_{vb} \approx J_c(L_c/a_0)^{27/5}$ in the large-bundle pinning limit [23]. The quantity L_c is less temperature dependent than J_c below the vortex-solid melting temperature T_M, and therefore $J_{vb} \propto J_c$ is approximately valid for $T < T_M$, consistent with our data in figure 3(b). Furthermore, the empirical result $J_{vb}(T) > J_c(T)$ for all fields suggests that $L_c < a_0$ in low fields and $L_c > a_0$ in high fields.

5. Current-driven vortex dynamics

To understand the current-driven vortex dynamics at different temperatures, we consider the correlation between the $\rho(T)$ and $J_c(T)$ data in figures 3(a) and 3(b). We note that $J_c(T)$ first decreases with increasing temperature, and then begins a sharp upturn at the 'predominantly coherent motion temperature' T_{pc} (to be elaborated later) where $\rho(T)$ is at a local maximum value, reaching a peak value at the 'plastic motion temperature' T_{pl} where $\rho(T)$ dips to a local minimum, and finally decreases rapidly to zero at approximately the thermodynamic temperature T_M [3] in the small-current limit ($J < 10^3$ A m^{-2}).

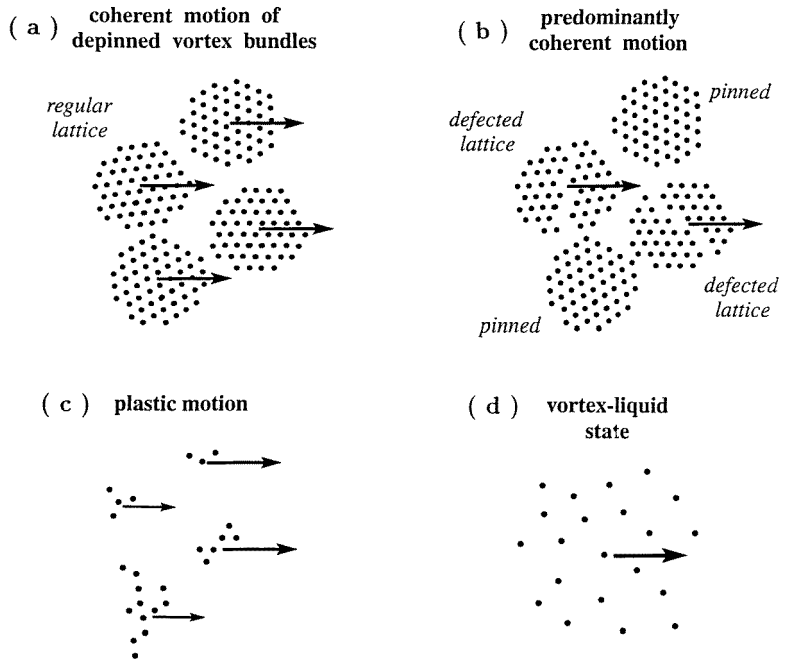

Figure 4. Schematic illustrations of the suggested current-driven vortex-bundle motion in various temperature regions. With increasing temperature, the vortex motion begins with (a) coherent motion of depinned vortex bundles, and then (b) becomes predominantly coherent motion with a defected lattice. Further increase of temperature leads to (c) plastic motion, and eventually (d) the vortex-liquid state before conversion into the normal state. We note that the possible dimensional crossover along the direction of $\boldsymbol{H}$ is not explicitly illustrated.

On the basis of the experimental information, we propose the following scenario for the different regimes of current-driven vortex dynamics. For $T < T_{pc}$, the presence of an external current density $J \gg J_c$ results in coherent motion of depinned vortex bundles [27] and therefore finite resistivity. The coherently moving bundles consist of a nearly

regular vortex lattice because the large applied current effectively 'heals' the defect-induced inhomogeneous vortex structure, as illustrated in figure 4(a). As the temperature increases to $T_{pc} < T < T_{pl}$, the moving vortex bundles become increasingly softened due to the rapidly decreasing c_{66} [15, 20], and therefore may be partially pinned by local defects [15, 20], resulting in the onset of plasticity with smaller and defected vortex bundles which undergo predominantly coherent motion [28], as illustrated in figure 4(b). The occurrence of partially pinned vortex bundles gives rise to an increasing J_c (the peak effect) and therefore decreasing vortex dissipation. With further increase of the temperature, the increasing plastic motion of vortices at $T > T_{pl}$ involves continuing break-ups of vortex bundles, as shown in figure 4(c). Therefore the resistivity rises rapidly between T_{pl} and T_M [28]. Near the melting temperature ($T \rightarrow T_M^-$), the root mean square amplitude of the vortex-lattice displacement $\sqrt{\langle u^2 \rangle}$ approaches the Lindemann criterion, $\sqrt{\langle u^2 \rangle} \sim c_L a_0$, where c_L is the Lindemann constant [2]. Thus, a vortex-solid melting transition takes place at T_M, above which in the vortex-liquid state (figure 4(d)) both the long-range shear modulus c_{66} and the critical current density J_c vanish. The resistivity continues to rise above T_M until vortex fluctuations associated with the melting transition subside, and the resistivity becomes independent of the current at a temperature T_{lin} slightly above T_M.

The above description of the current-induced vortex dynamics only focuses on the qualitative two-dimensional behaviour of vortex bundles. If we compare the temperature dependence of the longitudinal vortex correlation length L_c with the sample thickness d, an interesting dimensional crossover in the vortex correlation may occur, as predicted by the following consideration. Since L_c is related to the transverse correlation length R_c via the relation $L_c \approx R_c(c_{44}/c_{66})^{1/2}$, and since c_{66} vanishes at the melting transition line of untwinned $YBa_2Cu_3O_7$ single crystals [1–3] and at the glass transition line of twinned $YBa_2Cu_3O_7$ single crystals [29, 30], while the tilt modulus c_{44}, although significantly reduced in this regime [31], remains finite until $T \rightarrow T_c^-$, we find that c_{66} decreases more rapidly than c_{44} near T_M. Hence, a dimensional crossover of the vortex correlation is likely to occur slightly below T_M and near the peak of $J_c(T)$, from a three-dimensional vortex correlation with $L_c < d$ at low temperatures to a two-dimensional correlation with $L_c > d$ at high temperatures. This conjecture of dimensional crossover associated with the longitudinal vortex correlation [21] is complementary to the varying vortex dynamics from coherent vortex motion to plastic motion.

By plotting in the H–T diagram the characteristic temperatures T_{pc}, T_{pl} and T_{lin} for different fields, together with the thermodynamic vortex-solid melting transition temperature T_M, we find that all three curves for $H_{pc}(T)$, $H_{pl}(T)$ and $H_{lin}(T)$ in figure 5 converge to the thermodynamic melting line $H_M(T)$ in high fields, although in the low-field limit the peak effect is found to occur at temperatures substantially (more than 0.5 K) lower than T_M. The convergence of $H_{pc}(T)$, H_{pl} and $H_M(T)$ in high fields is consistent with the stronger elasticity and larger vortex bundles which minimize the occurrence of plastic motion.

6. Bulk pinning and the onset of plastic motion

Next, we consider the quantity $\rho_0(T)$ at $T \leqslant T_{pc}$, which corresponds to the dissipation associated with the coherent motion of completely depinned vortex bundles in the high-current limit, $\lim_{J \gg J_c}[\rho(T)] \rightarrow \rho_0(T)$. We note that the resistivity $\rho(T)$ for a given current density $J > J_c$ is nearly constant for $T \leqslant T_{pc}$, and $\rho(T)$ decreases rapidly above T_{pc}, where T_{pc} is the onset of plasticity, while the vortex motion is still predominantly coherent [28]. Therefore $\rho_0(T_{pc})$ may be considered as the maximum resistivity associated with the

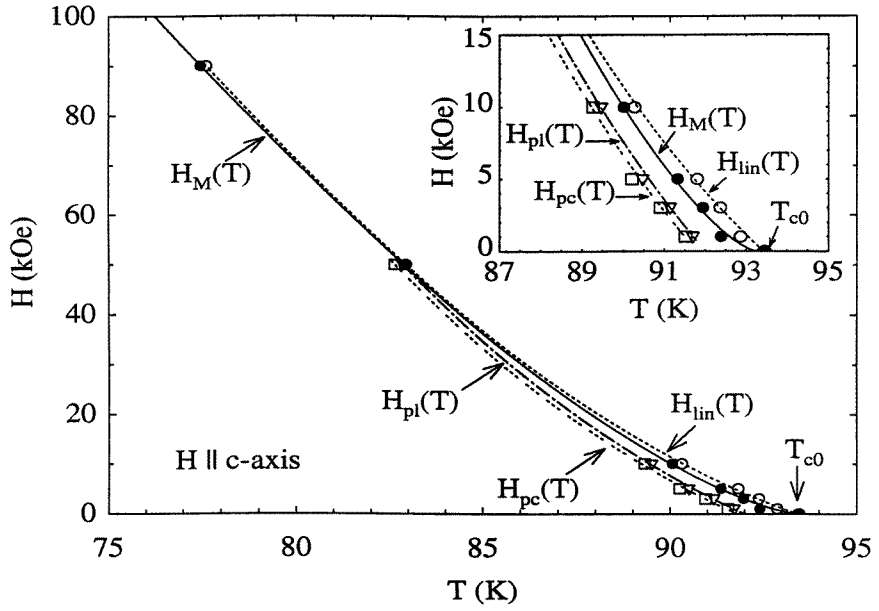

Figure 5. The H–T vortex phase diagram showing the thermodynamic phase transition line $H_M(T)$ and various other crossover lines $H_{pc}(T)$, $H_{pl}(T)$ and $H_{lin}(T)$. The inset shows a close-up view of the phase diagram in the lower-field limit, with various vortex regimes as indicated.

coherent motion of completely depinned vortex bundles. The current density required to maximize the resistivity is the plastic current density $J_p = c_{66}/(Br_p)$ [15], with r_p being the average separation of the point defects, and B the magnetic induction. Assuming a vortex drift velocity v, we may express the maximum resistivity at T_{pc} by the following formula (in CGS units):

$$\rho_0(T_{pc}) \approx \frac{vB}{J_p c} = \frac{vB^2 r_p}{c_{66} c}. \tag{2}$$

The physical significance of ρ_0 suggested in equation (2) may be verified by considering the magnetic field and angular dependence of $\rho_0(T_{pc})$. We may assume that the current required to induce the onset of plastic motion is predominantly determined by the hard-axis shear modulus $c_{66}^{\perp}(\theta) = c_{66}^0/\varepsilon_\theta$ [32], where $\varepsilon_\theta = \sqrt{\cos^2\theta + \varepsilon^2 \sin^2\theta}$, ε^2 is the mass anisotropy ratio defined as $\varepsilon^{-2} \equiv (m_c/m_{ab})$ [23, 33], and $c_{66}^0 \approx \Phi_0 B/(8\pi\lambda)^2 \sim B[1 - (T/T_c)]$. (We note that the mean-field expression for c_{66}^0 is used here, because we are considering the dynamic process of vortex depinning in the large-current limit. This consideration is different from that for the thermodynamic melting transitions, where the shear modulus under thermal equilibrium should be renormalized by the thermal fluctuations and should vanish at T_M rather than T_c.) Next, the drift velocity v may be approximated by $v \propto [H_{c2}(T,\theta)]^{-1}$, similarly to in the Bardeen–Stephen model [34], so $v \sim \varepsilon_\theta[1 - (T/T_c)]^{-1}$ because $H_{c2}(\theta) \propto \varepsilon_\theta^{-1}$ [23]. Thus, we find that the saturation resistivity at T_{pc} follows

$$\rho_0 \propto \frac{H\varepsilon_\theta^2}{[1 - (T_{pc}/T_c)]^2}$$

where $B \approx H$ has been assumed.

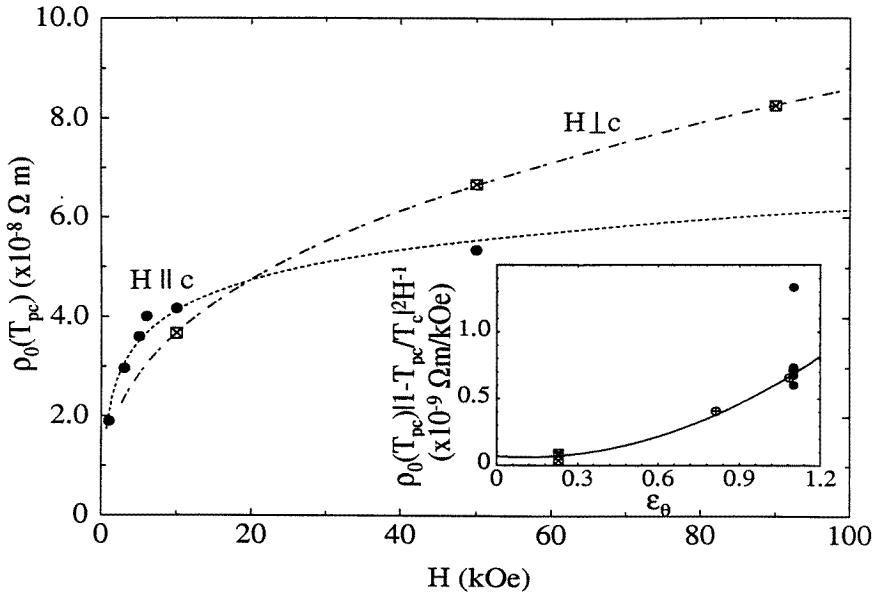

Figure 6. The magnetic field dependence of ρ_0 is shown for both $\boldsymbol{H} \parallel \hat{\boldsymbol{c}}$ and $\boldsymbol{H} \perp \hat{\boldsymbol{c}}$. The inset demonstrates the empirical relation $\rho_0(T_{pc})H^{-1}[1-(T_{pc}/T_c)]^2 = \alpha_0 + \alpha_1\varepsilon_\theta^2$ that approximately accounts for most data taken at different magnetic fields (H) and angles (θ).

The magnetic field and angular dependences of ρ_0 are shown in figure 6. We find that ρ_0 for most fields and angles follows a similar behaviour, as illustrated in the inset of figure 6 where all $\rho_0(H,\theta)$ data approximately satisfy the generalized empirical relation $\rho_0(T_{pc})H^{-1}[1-(T_{pc}/T_c)]^2 = \alpha_0 + \alpha_1\varepsilon_\theta^2$, and the fitting parameters are $\alpha_0 \approx 1.57\times10^{-10}$ Ω m kOe^{-1} and $\alpha_1 \approx 6.29\times10^{-10}$ Ω m kOe^{-1}. We remark that our estimate made using equation (2) for $\rho_0(T_{pc})$ is only approximate, especially with uncertainties in the drift velocity v. This uncertainty may be responsible for the additional angle-independent term α_0, as well as the deviation of one ρ_0-value from the empirical relation $\rho_0(T_{pc})H^{-1}[1-(T_{pc}/T_c)]^2 = \alpha_0 + \alpha_1\varepsilon_\theta^2$ in the high-field limit. However, we consider the general agreement of equation (2) with most $\rho_0(H,\theta)$ data reasonable support for the onset of plastic motion at T_{pc}.

7. Effects of high-density random point defects

In the previous sections we have studied the current-driven vortex dynamics in the limit of weak point disorder in an untwinned $YBa_2Cu_3O_7$ single crystal. It appears that the weak point disorder contributes to collective pinning of vortex bundles, as manifested by the occurrence of the peak effect under large currents, and by the diverging energy barrier for vortex motion in the low-current limit. Furthermore, the disorder is sufficiently weak that the vortex-solid–liquid phase transition has been found to be first order [1–3, 8–10, 13]. A natural follow-up is to investigate whether increasing point disorder eventually leads to a thermodynamically stable 'vortex-glass' state at low temperatures, with a vanishing resistivity in the low-current limit and a second-order glass-to-liquid transition at a finite temperatures below the $H_{c2}(T)$ line [11]. This approach is in contrast to those followed in previous reports of second-order 'vortex-glass' transitions in both twinned $YBa_2Cu_3O_7$

single crystals [29, 30] and thin films [35], in which stronger pinning defects other than the random point disorder may be much more important and ultimately responsible for the observed second-order, glassy vortex phase transitions.

The effects of large point disorder are studied by subsequently irradiating the same untwinned single crystal with 3.0 MeV protons using a fluence of 5×10^{15} protons cm^{-2}. As stated earlier, this irradiation condition created point and small-cluster defects of a volume density $n_p \sim (3 \times 10^{-8}\ \mathrm{m})^{-3}$ [24, 25]. After proton irradiation, we find neither a peak effect at high currents (see figure 7) nor resistive hysteresis at low currents. Furthermore, the corresponding E–J isotherms, as shown in the inset for the representative data in figure 7 taken at $H_{\|c} = 50$ kOe, are mostly ohmic for the entire temperature range and for all currents. Such an observation disagrees with the vortex-glass hypothesis [12] which asserts that a true low-temperature thermodynamic glassy phase characterized by a vanishing resistivity appears in the small-applied-current limit.

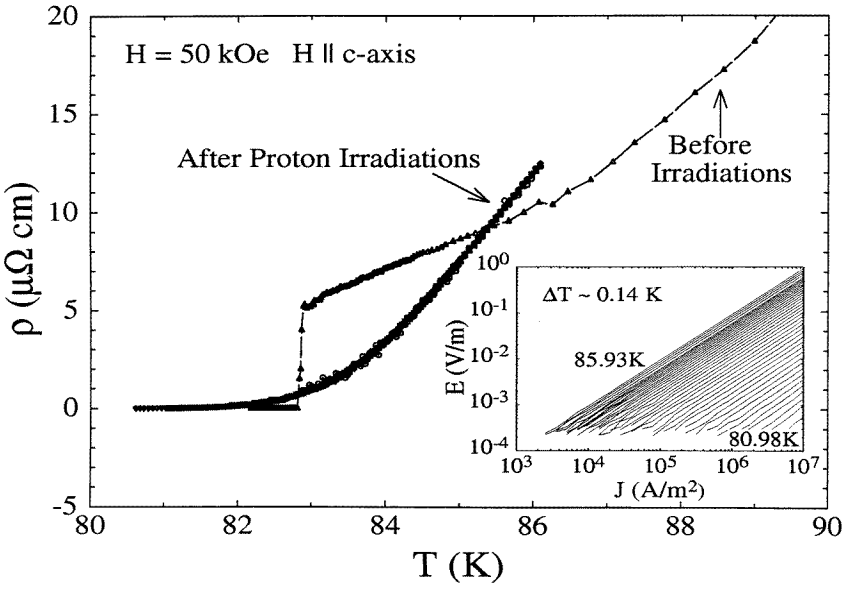

Figure 7. Comparison of the ohmic ρ versus T curves of the untwinned $YBa_2Cu_3O_7$ single crystal before and after 3 MeV proton irradiation. Note that the nearly completely ohmic behaviour after irradiation, shown in the inset, is in sharp contrast to the significantly non-linear E–J isotherms in figure 2 before irradiation. The averaged temperature increment of two consecutive isotherms in the inset is $\Delta T = 0.14$ K.

To yield a better quantitative understanding of the disappearance of non-linear current–voltage characteristics after proton irradiation of the single crystal, we perform the following analyses which consider the reduction of the vortex correlation lengths as the result of high-density point defects after proton irradiation. By comparing various characteristic lengths of vortices with the disorder characteristic length L_c^c [23], we shall argue that the vortex pinning mechanism in the proton-irradiated sample involves single-vortex pinning [23]. However, we find that the observed experimental E–J data cannot be explained with either the $E(J)$ behaviour quantitatively predicted by the collective flux-creep theory in the single-vortex pinning limit, or by the current dependence qualitatively proposed on the basis of the vortex-glass scenario [11].

Let us first consider the disorder characteristic length L_c^c for a given disorder parameter γ which is determined by the strength f_{pin} and density n_p of the pinning sites [23]:

$$L_c^c \approx \left[\left(\frac{\Phi_0}{4\pi\lambda}\right)^2 \xi\varepsilon^2\right]^{2/3} \Big/ \gamma^{1/3} \qquad \gamma \approx f_{pin}^2 n_p \xi^2 \tag{3}$$

where f_{pin} is the pinning force, and λ is the magnetic penetration depth. If we further assume that the pinning force per point defect can be approximated by the spatial variation of the condensation energy in a volume ξ^3 over a distance $\sim\xi$, so that $f_{pin} \approx (H_c^2\xi^2)$, and use the empirical value $n_p^{-1/3} \approx 30$ nm, as well as the material parameters for $YBa_2Cu_3O_7$: $\xi(0) = 1.2$ nm, $\lambda(0) = 140$ nm, $\varepsilon^{-2} = 60$ [36], we obtain $L_c^c \approx \varepsilon^{4/3}(4n_p)^{-1/3} \approx 1.2$ nm. Thus, L_c^c is approximately equal to the CuO_2 layer separation $d \approx 1.2$ nm in $YBa_2Cu_3O_7$, and is much smaller than the quantity εa_0 for all fields (up to 90 kOe) accessible in our experiments. It has been argued [23] that the vortex system is in the single-vortex pinning regime if $L_c^c < \varepsilon a_0$, and therefore the L_c^c-value of our proton-irradiated untwinned single crystal is consistent with this criterion.

The critical current density in the single-vortex pinning regime can be estimated from the expression $J_c \approx J_0(\varepsilon\xi/L_c^c)^2 \equiv J_{sv}$ [23]. Hence, for temperatures of $\sim 0.9T_c$, we obtain $J_c \sim 10^{10}$ A m^{-2}, which is much larger than the current densities accessible in our experiments. The condition $J \ll J_c \approx J_{sv}$ is therefore satisfied for our measurements, and the corresponding prediction for $E(J)$ yields $E \propto \exp[-U(J)/(k_BT)]$, where $U(J) \equiv U_{vb}(J_{vb}/J)^\mu$, and the quantities of U_{vb}, J_{vb} and μ are positive constants dependent on the range of vortex correlation [23]. In the context of collective flux-creep theory, we consider the values of μ and J_{vb} for the experimentally relevant current range between 10^3 and 10^7 A m^{-2} by first defining the characteristic current densities for the single-vortex (sv), small-bundle (sb), large-bundle (lb) and charge-density-wave (CDW) regimes [23]:

$$\begin{aligned} J_{sv} &\approx J_0\left[\frac{\varepsilon\xi}{L_c^c}\right]^2 \qquad & J_{sb} &\approx J_{sv}\left[\frac{L_c^c}{\varepsilon a_0}\right]^{7/5} \\ J_{lb} &\approx J_{sb}\left[\frac{\varepsilon a_0}{\lambda}\right]^2 \qquad & J_{\mathrm{CDW}} &\approx J_{lb}\left[\frac{\varepsilon^3\xi^5}{a_0^2(L_c^c)^3}\right]^{9/5}. \end{aligned} \tag{4}$$

For $T = 0.91T_c$ and $H = 50$ kOe, we find that $J_{vb} = J_{sb}$ and $\mu = 3/4$ if the applied current density satisfies the condition $J_{lb} < J < (a_0/\lambda)^2 J_{sb}$ [23], where the characteristic currents are estimated as $J_{lb} \sim 10^5$ A m^{-2} and $(a_0/\lambda)^2 J_{sb} \sim 10^7$ A m^{-2}. Similarly, $J_{vb} = J_{\mathrm{CDW}}$ and $\mu = 1/2$ if $0 < J < J_{\mathrm{CDW}}$ [23], where $J_{\mathrm{CDW}} \sim 10^4$ A m^{-2}. Consequently, we find that over the entire experimental current range, the functional forms of $E(J)$ as predicted by the collective flux-creep theory all assume non-linear and diverging energy barriers $U(J)$ for $J \ll J_c$, in sharp contrast to our experimental data shown in figure 7. Furthermore, within our voltage resolution there is no evidence in the E–J isotherms for a second-order vortex-glass transition [11] in this proton-irradiated untwinned $YBa_2Cu_3O_7$ single crystal, in contrast to the E–J isotherms in thin films [35] and twinned crystals of $YBa_2Cu_3O_7$ [29, 30], which exhibit diverging $U(J)$ at low temperatures, power-law dependence near the glass transition temperature, and thermally activated flux-flow (TAFF) behaviour above the glass transition and below the H_{c2}-line [29, 30, 35]. We also note that for the twinned $YBa_2Cu_3O_7$ single crystals, consistent experimental evidence of second-order glass transitions has been manifested in measurements of the complex conductivity and magnetic susceptibility [30], in addition to the E–J isotherms [29, 30]. Such consistent manifestation of second-order glass transitions is *not* observed for the *untwinned* $YBa_2Cu_3O_7$ single crystal.

Although neither collective flux-creep theory nor the vortex-glass scenario can explain the current–voltage characteristics of the data for the proton-irradiated untwinned $YBa_2Cu_3O_7$ single crystal, we remark that in the context of single-vortex pinning due to large point disorder, the absence of resistive peaks below T_M may be understood by noting that in the single-vortex pinning regime, individual vortices are either pinned or completely depinned, so plastic motion which involves break-ups of vortex bundles cannot occur. Thus, the peak effect associated with softening of vortex bundles below T_M is not observed in the presence of strong pinning and/or high-density point defects. Our experimental results for the proton-irradiated untwinned $YBa_2Cu_3O_7$ single crystal therefore suggest that the resistive peak effect originates in the motion of softened vortex bundles below T_M for systems with weak pinning and small elasticity.

According to equation (3), the disorder characteristic length L_c^c decreases with increasing point disorder. Hence, collective motion of three-dimensionally correlated vortex bundles with a diverging energy barrier $U(J) \propto J^{-\mu}$ ($\mu > 0$) may be achieved if the point disorder density (n_p) is reduced. However, we caution that the presence of a diverging energy barrier at low temperatures, although suggestive, is not a sufficient condition for the existence of a second-order vortex-glass transition. We also note that earlier reports of experimental evidence for vortex-glass transitions in thin films [35] and twinned single crystals of $YBa_2Cu_3O_7$ [29, 30] may be largely associated with correlated disorder, such as twin planes or screw dislocations, rather than random point disorder in the samples. The significant differences between the 'vortex-glass' critical exponents for twinned $YBa_2Cu_3O_7$ single crystals [29, 30] and those for $YBa_2Cu_3O_7$ epitaxial films [35] are strongly suggestive of different universality classes of vortex phase transitions due to different types of correlated disorder. It is likely that the second-order vortex phase transitions observed in $YBa_2Cu_3O_7$ epitaxial films [35] are in fact Bose-glass transitions incurred by line disorder such as screw dislocations [12], whereas those in $YBa_2Cu_3O_7$ single crystals [29, 30] are XY-like transitions due to the twin planes [37].

8. Comparison with other related experiments

Comparing with previous reports of resistive peaks in similar systems [5, 6, 21], we note the following new aspects of this work. First, our quantitative analysis of the E–J characteristics in the as-grown untwinned $YBa_2Cu_3O_7$ single crystal provides evidence for the motion of vortex bundles with finite elastic moduli, and the physical origin of the peak effect is attributed to the motion of softened vortex bundles below the thermodynamic melting transition T_M. Various types of current-driven vortex dynamics at $T < T_M$ are proposed, and the possibility of an accompanying dimensional crossover in the vortex correlation is also discussed in the context of the different temperature variations in c_{66} and c_{44} near T_M. The latter viewpoint of a dimensional crossover near the occurrence of the peak effect is analogous, but not identical, to that described in reference [21]. Second, the general agreement of the angular and magnetic field dependence of ρ_0 with equation (2) provides further quantitative support for the existence of current-driven plastic motion below T_M. Finally, the effects of a large degree of point disorder on the vortex phases and dynamics of untwinned $YBa_2Cu_3O_7$ single crystals are also investigated and compared with the collective flux-creep theory and vortex-glass scenario. We have shown that for a sufficiently large density of point defects, the vortex correlation is significantly reduced, and the vortex system at low temperatures may be characterized as in the single-vortex pinning regime. In contrast to the case for the as-grown untwinned crystal, we find neither resistive hysteresis at low currents nor a peak effect at high currents for the sample after proton irradiation.

Furthermore, the current–voltage characteristics at all temperatures below T_c appear to be ohmic, even for applied current densities much smaller than the theoretically predicted J_c (see section 7). This finding is in contrast to the diverging energy barrier for vortex motion based on either the collective flux-creep theory [23] or the point-disorder-induced vortex-glass model [11]. The puzzling low-temperature ohmic current–voltage characteristics for the sample with a large degree of point disorder seem to suggest that the vortex system for a high density of point defects cannot form a stable vortex-solid phase, at least in the presence of finite applied currents. In other words, the system appears to be liquid-like, with a negligible—if there is any—critical current density, so the E–J data appear to be in the flux-flow regime for all experimentally accessible currents. Although we cannot rule out the possibility of a stable vortex-glass phase at much lower temperatures and/or under much smaller applied currents, the discrepancy between the theoretical J_c and our observation of ohmic behaviour at $J \ll J_c$ for the proton-irradiated untwinned $YBa_2Cu_3O_7$ suggests the need for further theoretical and experimental studies in order to resolve this issue.

9. Conclusion

In summary, we have investigated the current-driven vortex dynamics of an untwinned $YBa_2Cu_3O_7$ single crystal under different densities of point disorder and over a broad range of temperature, magnetic field strength and orientation, and current density. For the as-grown untwinned sample which is in the weak-pinning limit, non-linear resistive peaks are observed at $J > J_c$. These resistive peaks are found to be correlated with the peak effect in the critical current density (J_c) below the vortex-solid melting transition. In addition, the current–voltage characteristics in the same temperature range are analysed and are found to be consistent with the collective flux-creep model for the motion of vortex bundles. With increasing temperature, the resistive peak effect can be understood in terms of a current-driven coherent vortex motion at lower temperatures, followed by a decrease in dissipation due to partial pinning of softened vortex bundles, then a rapid rise in the dissipation due to plastic vortex motion, and finally a thermally induced melting transition above which the shear modulus vanishes. Comparing our results with similar observations for various superconducting systems, we conclude that the peak effect is a current-induced phenomenon common in both conventional type-II and high-temperature superconductors.

We have also investigated the effects of high-density random point defects on the current-driven vortex dynamics through proton irradiation of an untwinned $YBa_2Cu_3O_7$ single crystal. We find that neither resistive hysteresis at low currents nor a peak effect at high currents exists after proton irradiation. Furthermore, we find that within our experimental resolution, there is no visible energy barrier to vortex motion, in sharp contrast to the vortex-glass scenario which asserts a point-disorder-induced stable-thermodynamics vortex phase with a diverging energy barrier in the low-current limit. Comparing this finding with previous reports of 'vortex-glass' transitions in $YBa_2Cu_3O_7$ twinned single crystals [29, 30] and epitaxial films [35] (including our own work on $YBa_2Cu_3O_7$ twinned single crystals [30] which consistently manifested the same class of second-order glass transitions in measurements of the current–voltage characteristics, complex conductivity, and magnetic susceptibility), we conjecture that the high-density point defects, in the absence of other correlated disorder, may result in a low-temperature liquid-like state which is unstable against finite applied currents. Although it is possible that a thermodynamically stable vortex-glass phase may exist at much lower temperatures and/or under applied currents much smaller than those used in our measurements, the experimental data reported in this

work on a proton-irradiated untwinned $YBa_2Cu_3O_7$ single crystal clearly indicate that the critical current of the vortex glass, if exists, is much smaller than the theoretical prediction. This finding calls for further investigation of the current-driven vortex dynamics of extreme type-II superconductors.

Acknowledgments

The authors are grateful to Dr V M Vinokur, Dr A V Samoilov and Dr M Konczykowski for useful discussions. This work was jointly supported by NSF Grants No DMR-9401315 and No DMR93-18931, ONR Grant No N00014-91-J-1556, the David and Lucile Packard Foundation, and NASA.

References

[1] Safar H, Gammel P L, Huse D A, Bishop D J, Rice J P and Ginsberg D M 1992 *Phys. Rev. Lett.* **69** 824
Safar H, Gammel P L, Huse D A, Bishop D J, Lee W C and Ginsberg D M 1993 *Phys. Rev. Lett.* **70** 3800
[2] Kwok W K, Fendrich J, Fleshler S, Welp U, Downey J and Crabtree G W 1994 *Phys. Rev. Lett.* **72** 1092
Kwok W K, Fendrich J, Welp U, Fleshler S, Downey J and Crabtree G W 1994 *Phys. Rev. Lett.* **72** 1088
[3] Jiang W, Yeh N-C, Reed D S, Kriplani U and Holtzberg F 1995 *Phys. Rev. Lett.* **74** 1438
[4] Bhattacharya S and Higgins M J 1993 *Phys. Rev. Lett.* **70** 2617
[5] Ling X and Budnick J I 1991 *Magnetic Susceptibility of Superconductors and Other Spin Systems* ed R A Hein *et al* (New York: Plenum) p 377
[6] Kwok W K, Fendrich J A, van der Beek C J and Crabtree G W 1994 *Phys. Rev. Lett.* **73** 2614
[7] D'Anna G, Indenbom M V, Andre M O, Benoit W and Walker E 1994 *Europhys. Lett.* **25** 225
[8] Welp U, Fendrich J A, Kwok W K, Crabtree G W and Veal B W 1996 *Phys. Rev. Lett.* **76** 4809
Fendrich J A, Welp U, Kwok W K, Koshelev A E, Crabtree G W and Veal B W 1996 *Phys. Rev. Lett.* **77** 2073
[9] Zeldov E, Majer D, Konczykowski M, Geshkenbein V B, Vinokur V M and Shtrikman H 1995 *Nature* **375** 373
[10] Schilling A, Fisher R A, Phillip N E, Welp U, Dasgupta D, Kwok K and Crabtree G W 1996 *Nature* **382** 791
[11] Fisher D S, Fisher M P A and Huse D A 1991 *Phys. Rev.* B **43** 130
[12] Nelson D R and Vinokur V M 1992 *Phys. Rev. Lett.* **68** 2398
Nelson D R and Vinokur V M 1993 *Phys. Rev.* B **48** 13 060
[13] Hetzel R E, Sudbø A and Huse D A 1992 *Phys. Rev. Lett.* **69** 518
[14] Hwa T, Nelson D R and Vinokur V M 1993 *Phys. Rev.* B **48** 1167
[15] Larkin A I, Marchetti M C and Vinokur V M 1995 *Phys. Rev. Lett.* **75** 2992
[16] Nguyen A K, Sudbø A and Hetzel R E 1996 *Phys. Rev. Lett.* **77** 1592
[17] DeSorbo W 1964 *Rev. Mod. Phys.* **36** 90
[18] Wördenweber R, Kes P H and Tsuei C C 1986 *Phys. Rev.* B **33** 3172
[19] Pippard A B 1969 *Phil. Mag.* **19** 217
[20] Larkin A I and Ovchinnikov Yu N 1979 *J. Low Temp. Phys.* **34** 409
[21] Solovjov V F, Pan V M and Freyhardt H C 1994 *Phys. Rev.* B **50** 13 724
Pan V M, Solovjov V F, Svetchnikov and Freyhardt H C 1995 *IEEE Trans. Appl. Supercond.* **5** 1892
Pan V M, Solovjov V F and Freyhardt H C 1996 *Czech. J. Phys. Suppl.* S3 **46** 1643
[22] Feigel'man M V, Geshkenbein V B, Larkin A I and Vinokur V M 1989 *Phys. Rev. Lett.* **63** 2303
[23] Blatter G, Feigel'man M V, Geshkenbein V B, Larkin A I and Vinokur V M 1994 *Rev. Mod. Phys.* **66** 1125
[24] Jiang W, Yeh N-C, Reed D S, Kriplani U, Tombrello T A, Rice A P and Holtzberg F 1993 *Phys. Rev.* B **47** 8308
[25] Thompson M W 1969 *Defects and Radiation Damage in Metals* (Cambridge: Cambridge University Press)
[26] Fisher D S 1985 *Phys. Rev.* B **31** 1396
[27] We remark that the vortex motion at low temperatures may not always be coherent unless the pinning is weak. A plastic flow is possible if strong and localized pinning sites exist and if the applied current density is only slightly larger than J_c.

[28] The predominantly coherent motion of vortex bundles between T_{pc} and T_{pl} is a special case of the plastic motion. Similar to ice motion in a river in early spring (called 'ledohod' in Russian), this type of vortex dynamics involves break-ups of coherently moving vortex bundles. Above T_{pl} and below T_M, the plastic motion of vortex bundles becomes incoherent and the bundles continue to break into smaller fragments.
[29] Gammel P L, Bishop D J and Schneemeyer L F 1991 *Phys. Rev. Lett.* **66** 953
[30] Yeh N-C, Jiang W, Reed D S, Kriplani U and Holtzberg F 1993 *Phys. Rev.* B **47** 6146
Reed D S, Yeh N-C, Jiang W, Kriplani U and Holtzberg F 1993 *Phys. Rev.* B **47** 6150
Reed D S, Yeh N-C, Jiang W, Kriplani U, Beam D A and Holtzberg F 1994 *Phys. Rev.* B **49** 4384
Yeh N-C, Jiang W, Reed D S, Kriplani U, Konczykowski M, Tombrello T A, Holtzberg F and Tsuei C C 1996 *Ferroelectrics* **177** 143
[31] Sudbø A and Brandt E H 1991 *Phys. Rev. Lett.* **66** 1781
[32] Kogan V G and Campbell L J 1989 *Phys. Rev. Lett.* **62** 1552
[33] Blatter G, Geshkenbein V B and Larkin A I 1992 *Phys. Rev. Lett.* **68** 875
[34] Bardeen J and Stephen M J 1965 *Phys. Rev.* **140** A1197
[35] Koch R H, Foglietti V, Gallagher W J, Koren G, Gupta A and Fisher M P A 1989 *Phys. Rev. Lett.* **63** 1151
[36] Beck R G, Farrell D E, Rice J P, Ginsberg D M and Kogan V G 1992 *Phys. Rev. Lett.* **68** 1594
[37] Balents L and Nelson D R 1994 *Phys. Rev. Lett.* **73** 2618
Balents L and Nelson D R 1995 *Phys. Rev.* B **52** 12 951